Review of Scientific Instruments

Rapidly frequency-tuneable, in-vacuum, and magnetic levitation chopper for fast modulation of infrared light

Cite as: Rev. Sci. Instrum. **93**, 085105 (2022); https://doi.org/10.1063/5.0097279
Submitted: 27 April 2022 • Accepted: 14 July 2022 • Published Online: 15 August 2022

Ioannis Lekkas, Mark D. Frogley, Timon Achtnich, et al.

Review of Scientific Instruments ARTICLE scitation.org/journal/rsi

Rapidly frequency-tuneable, in-vacuum, and magnetic levitation chopper for fast modulation of infrared light

Cite as: Rev. Sci. Instrum. 93, 085105 (2022); doi: 10.1063/5.0097279
Submitted: 27 April 2022 • Accepted: 14 July 2022 •
Published Online: 15 August 2022

Ioannis Lekkas,[1] Mark D. Frogley,[1,a)] Timon Achtnich,[2] and Gianfelice Cinque[1]

AFFILIATIONS

[1] MIRIAM Beamline B22, Diamond Light Source Ltd., Harwell Science and Innovation Campus, Oxon OX11 0DE Chilton, Didcot, United Kingdom
[2] Celeroton AG, Industriestrasse 22, 8604 Volketswil, Switzerland

[a)] **Author to whom correspondence should be addressed:** mark.frogley@diamond.ac.uk

ABSTRACT

We present an in-vacuum mechanical chopper running at high speed and integrated into a magnetic levitating motor for modulating optical beams up to 200 kHz. The compact chopper rotor allows fast acceleration (10 kHz s^{-1} as standard) for rapid tuning of the modulation frequency, while 1 mm diameter slots provide high optical throughput for larger infrared beams. The modulation performances are assessed using a reference visible laser and the high brightness, broadband, infrared (IR) beam of synchrotron radiation at the MIRIAM beamline B22 at Diamond Light Source, UK. For our application of IR nanospectroscopy, minimizing the temporal jitter on the modulated beam due to chopper manufacturing and control tolerances is essential to limit the noise level in measurements via lock-in detection, while high modulation frequencies are needed to achieve high spatial resolution in photothermal nanospectroscopy. When reaching the maximum chopping frequency of 200 kHz, the jitter was found to be 0.9% peak-to-peak. The described chopper now replaces the standard ball-bearing chopper in our synchrotron-based FTIR photothermal nanospectroscopy system, and we demonstrate improved spectroscopy results on a 200 nm thickness polymer film.

I. INTRODUCTION

Amplitude modulation of optical beams has a broad range of applications, including time-resolved spectroscopy, low-noise optical measurements via lock-in amplification (where the signal of interest is shifted to a low-noise domain at the modulation frequency), and photothermal/photoacoustic spectroscopy and imaging, where the depth sensitivity in the sample depends on the modulation frequency. Some light sources can be directly amplitude-modulated, as in some laser systems, but for many other sources and some specific applications, external modulation—chopping—of the optical beam is required to achieve the desired modulation frequency and temporal pattern. A variety of light choppers has been introduced throughout the years, e.g., Refs. 1–22, including mechanical choppers with electrical motors, micro-electromechanical systems (MEMS) or in-vacuum choppers.

Ball-bearing DC motor choppers[1–3] can have good rotational stability, low jitter, and wide frequency tuneability, but only up to modest rotational frequencies. To achieve high modulation frequencies, a large number of smaller slots is, therefore, required and the jitter is then limited by the precision of mechanical machining of the slot size and position. A customized commercial system used in our laboratory (with a 200- or 400-slot disk in vacuum) allowed modulation up to 70 kHz with measured jitter above 2%.[1] Using brushless motors, 100 kHz modulation has been achieved with a 360-slot disk[2] and a system in vacuum demonstrated 120 kHz modulation at significantly higher rotational frequency using a 120-slot disk.[3] The need for smaller slots also limits the beam size that can be used, which constrains the spectral range at long wavelengths and/or the flux, especially for infrared sources. For effective modulation without aliasing, the full optical beam must be small enough to pass only through one slot at a time.[4]

Several kinds of MEMS choppers have been developed, mostly for application in miniature optical systems. One type[5] is bulk micromachined on a quartz substrate, which has a variety of advantages, including the etching of fine structures, use of piezoelectric properties for moving the chopper parts and as a detection mechanism, as well as the long lifetime of the quartz resonators. Other categories of MEMS devices include thin film optical choppers or comp actuators,[6,7] which allow various motions such as translational and rotational and can be fabricated to operate at specific frequencies.[8] Major limitations of MEMS choppers are the small displacement of the chopping element, typically 10–100 microns [not suitable for modulating large infrared (IR) beams] and the requirement to work at high quality-factor mechanical resonances of the device resulting in a very narrow frequency range for each design.[5–9] Typical modulation frequencies are up to a few kHz.

A different method, suitable for UHV application, employed a magnetically oscillated reed[10] for chopping a molecular beam (in this example at very low frequencies below 100 Hz). Like MEMS devices, this relies on mechanical resonances to achieve useful displacement of the chopping element and has very limited tuneability.

To achieve large range tuning of the modulation frequency, motor-based systems, therefore, remain an attractive approach. To avoid limitations due to ball-bearing friction, one development[11] used air bearings allowing rotation up to 30 krpm, limited by the yield strength of the large diameter disk (280 mm). With a disk of 45 slots, each 350 μm wide, a maximum modulation frequency of 22.6 kHz was achieved, but with an impressive jitter below 2 ns as required for the x-ray application.

The use of magnetic levitation bearings in vacuum motor choppers allows even greater reduction of friction to achieve exceptional performances. Several examples have been demonstrated with quite different designs for specific applications. Extremely high modulation frequencies up to 1.25 MHz were achieved[12] with a 1252 slotted disk designed for a small x-ray beam of just 70 μm size, yielding a stable but slowly tuneable modulation frequency. An early example of a magnetic levitation chopper[13] was designed for UHV use and lower frequency modulation (9 kHz) but with excellent stability for time-resolved tokamak plasma emission applications with 24 narrow (250 μm) slots in a large diameter disk (245 mm) to give a short transmission window (0.55 μs). Another magnetic bearing system[14] uses a rotating cylinder with the optical beam axis perpendicular to the rotation axis so the beam passes sequentially through two slots for a specific application of coincidence spectroscopy at up to 80 kHz. Finally, by using a triangular blade with a tunnel aperture,[15] a chopper with a very well-defined 300 ns transmission window for x-ray pulse-picking was achieved, requiring a 60 krpm rotational frequency, with just one modulation per revolution (1 kHz).

In this paper, we describe a novel in-vacuum, magnetic levitation chopper that is compact, is specifically designed for passing large diameter (1 mm) optical beams, and with high acceleration allowing rapid tuning of the modulation frequency up to 200 kHz.

In Sec. II, we describe and characterize the performances of the chopper, based on a magnetic levitation motor from Celeroton AG (Switzerland). Detailed performance measurements are presented, showing low jitter on the beam modulation at the highest modulation frequency of 200 kHz. Contributions to the jitter are discussed.

In Sec. III, we demonstrate the benefits of the new chopper in our IR nanospectroscopy application, where we time-modulate a quasi-continuous beam of spectrally ultra-broadband infrared synchrotron radiation to match the mechanical contact resonance frequencies of an atomic force microscope cantilever in contact with a polymer sample. This allows resonantly enhanced detection of minute (picometre) photothermal expansions of the sample caused by the absorption of IR light, which can be processed to obtain nanoscale IR absorption spectra of the sample.[1,23,24]

In Sec. IV, we summarize the paper and discuss further developments and applications.

II. MAGNETIC LEVITATION CHOPPER DESIGN AND PERFORMANCE

A. Magnetic levitation motor

The new chopper is a magnetic levitation motor with a customized rotor working as the chopper blade. Magnetic bearings have many advantages compared to conventional ball bearings, such as no friction and wear limits, reliability, and long lifetime. Magnetic bearings are based on contactless technology and can operate in-vacuum, avoiding air friction and allowing significantly higher rotational speeds. In contrast, for in-vacuum applications, ball bearings require a sealed atmosphere to contain lubricant outgassing.

The chopper motor for this experiment (CM-AMB-400 from Celeroton AG) consists of the dual hetero-/homopolar slotless/ironless self-bearing machine with integrated chopper rotor as shown in Fig. 1. The drive torque and the radial bearing forces are generated by the heteropolar motor, while the radial and the axial bearing forces are generated by the homopolar motor. A radial permanent magnet is embedded in the rotor sleeve on the heteropolar rotor side (visible in Fig. 1), while two axial magnets are employed in the homopolar rotor shaft. The maximum rotational speed depends on the minimization of losses in this system, and a slot-less design is best suited for high-speed applications.

To allow for the closed-loop control of all six degrees of freedom of the rotor, the radial rotor positions are measured by means of eddy-current sensors in both bearings. Additional Hall sensors in the

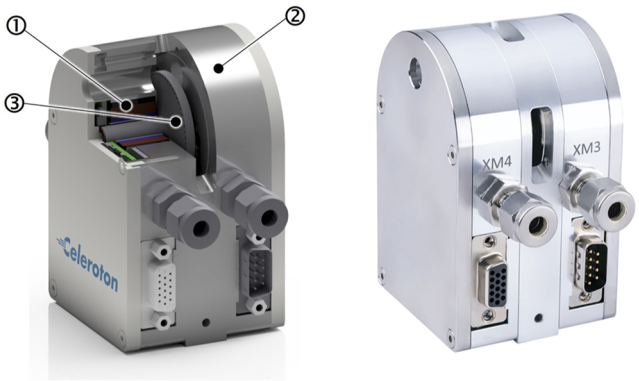

FIG. 1. Left: Cutaway view of chopper motor. ①: Heteropolar stator. ②: Homopolar stator. ③: Chopper rotor wheel. Right: Picture of the chopper motor.

heteropolar motor are used for measuring the axial rotor position and the rotor angle.

B. Chopper rotor wheel design

The chopper rotor wheel is designed to achieve a chopper frequency of up to 200 kHz. The 1 mm diameter hole was a requirement to avoid clipping of a long wavelength (far-IR) optical beam. The hole circle diameter is chosen such that the beam aligned through the chopper holes is approximately in the middle of the given stator opening, yielding 57 holes on the chopper rotor. The required nominal rotational frequency is, therefore, ~211 krpm to reach the chopper frequency of 200 kHz. The holes in the chopper rotor are manufactured by wire electrical discharge machining (EDM) to reach highest mechanical precision.

Figure 2 illustrates the simulated stress distribution on the chopper rotor at 211 krpm. The maximal stress develops at the transition from the hubs to the disk. It does not exceed 400 MPa and, therefore, has an adequate margin with respect to the tensile strength of titanium.

C. Jitter measurement and performances

For the measurement of the jitter, the collimated beam of a standard visible diode laser (FP-Mini-650 from Laser Components) was aligned with the holes of the chopper rotor and detected by a photodiode (SD 112-42-11-221 from LUNA Optoelectronics). Figure 3 depicts the setup, which is placed in a vacuum chamber at 1 mbar. The rotor was operated at the maximum safe rotational speed of 211 krpm, which corresponds to a chopper modulation frequency f_{chpr} of 200 kHz. The signal of the photodiode is measured with an oscilloscope (44MXi-A from LeCroy) in sequence mode, using a rising edge trigger on the waveform to generate the timestamps, t, of a long series of trigger signals, which are stored and processed afterward. The relative jitter, $J_{rel\cdot ppm}(n)$, between consecutive trigger signals is defined in parts per million with respect to f_{chpr},

$$\Delta t(n) = t(n+1) - t(n), \tag{1}$$

$$J(n) = \Delta t(n) - t_{ref} = \Delta t(n) - \frac{1}{f_{chpr}}, \tag{2}$$

$$J_{rel,ppm}(n) = \left(\Delta t(n) \cdot f_{chpr} - 1\right) \cdot 10^6. \tag{3}$$

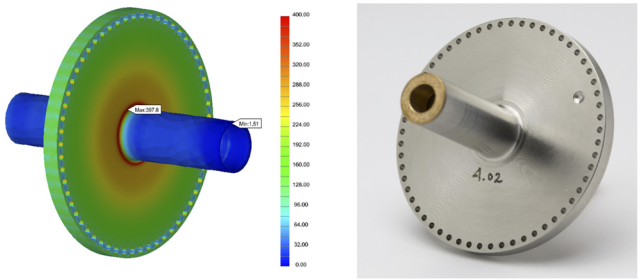

FIG. 2. Left: Stresses in MPa on rotor due to centrifugal force at 211 krpm. Right: Photo of a manufactured rotor.

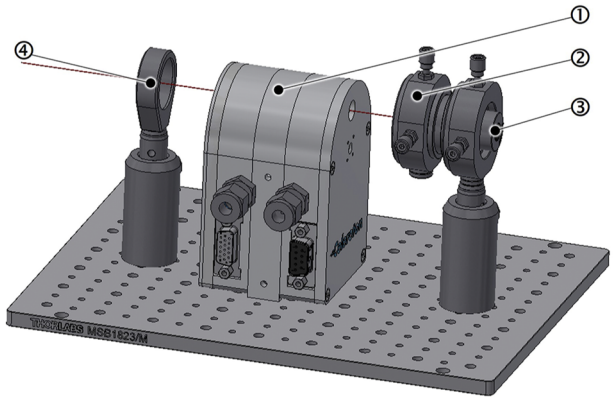

FIG. 3. Jitter test setup. ①: Magnetic bearing motor. ②: Precision 0.5 mm pinhole. ③: Laser. ④: Receiver diode.

For each of the 57 holes in the chopper rotor, denoted as k = 1 to 57, the statistics of the jitter over multiple revolutions is analyzed to separate the deterministic (repeating every rotation of the chopper) and random components of the jitter. The jitter per transition, J_{trans}, from hole k to the next hole is grouped according to

$$J_{trans}(\mathrm{k}, i) = J_{rel\cdot ppm}(\mathrm{k} + (i-1) \cdot N). \tag{4}$$

Here, i ranges from 1 to i_{max} and denotes the ith revolution and $N = 57$ is the total number of holes on the chopper rotor. The mean jitter for the kth transition is, then,

$$\bar{J}_{trans}(k) = \frac{\sum_{i=1}^{i_{max}} J_{trans}(k, i)}{i_{max}} \tag{5}$$

and the standard deviation is, thus, calculated using the expression

$$\sigma_{J_{trans}}(k) = \sqrt{\frac{\sum_{i=1}^{i_{max}} \left[J_{trans}(k, i) - \bar{J}_{trans}(k)\right]^2}{i_{max}}}. \tag{6}$$

We optically measured the jitter at modulation frequencies 50, 100, 150, and 200 kHz. The optical jitter measured for the frequency range 50–100 kHz was typically around 2% peak-to-peak, reducing to around 1% peak-to-peak at 150–200 kHz. We analyze here in detail the jitter performance at the highest frequency of 200 kHz. Several factors contribute to the overall jitter: the hole positioning on the rotor disk, the hole size tolerance, and the precision and stability of the orbit of the magnetically levitated rotor disk.

Figure 4 shows the relative jitter from every hole during 25 rotations while the chopper is spinning (at 211 krpm) with a modulation frequency of 200 kHz. The mean jitter per transition, $\bar{J}_{trans}$, the standard deviation of the jitter per transition $\sigma_{J_{trans}}$, and the peak-to-peak value of the jitter per transition $J_{trans,p-p}$ for every hole transition are plotted.

The data of Fig. 4 show a deterministic short-term drift (purple curve), which is periodic with the rotation. Furthermore, there is a deterministic jitter specific to each hole transition (blue curve). For

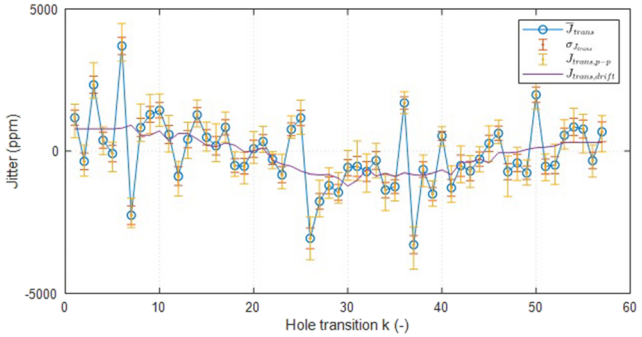

FIG. 4. Relative jitter for every hole transition measured over 25 turns at a modulation frequency of 200 kHz.

each hole transition, random jitter remains. The absolute peak-to-peak jitter is 0.9% as determined by the two worst-case transitions, 6 and 37.

For the potential further reduction of jitter, the classification of deterministic and random jitter is important. The short-term drift of Fig. 4 can be assigned to the residual noncongruency between the hole circle and the center of mass. At high rotational frequencies, the rotor is forced to rotate around the barycenter (center of mass), and not around the nominal geometrical center of the rotor. Therefore, the alignment of the hole circle precesses with respect to the stator and the IR beam. Attempts have been made to minimize this effect in the fine-tuning of the disk and control system. The systematic jitter seen for each specific hole transition (defined as $\bar{J}_{trans} - J_{trans,drift}$) is seen on every revolution and can be assigned to the manufacturing inaccuracy of the position and/or diameter of each hole. Finally, a residual level of random jitter is observed and may arise from the measurement inaccuracy or from random statistical fluctuations in the control system. The key finding is that the jitter performance is dominated by deterministic (rotor manufacture) tolerances rather than control, showing the potential for even better performances in future.

III. APPLICATION FOR SYNCHROTRON PHOTOTHERMAL NANOSPECTROSCOPY

A. Technique overview

Resonance-enhanced atomic force microscopy with synchrotron infrared light is an established method[1,23,24] where the light is focused at the AFM tip in contact with the sample. As the sample absorbs the chopper-modulated IR light, it thermo-mechanically expands and contracts at the modulation frequency. This expansion is detected as the AFM-IR signal via induced movement of the tip and the corresponding deflection of the AFM cantilever. The IR beam is further time-modulated by an FTIR spectrometer (before the chopper and sample), so the local nanoscale IR spectrum is encoded in the photothermal AFM-IR signal and can be recovered by conventional Fourier transform. By tuning the chopper modulation to a contact resonance of the cantilever, several orders of magnitude signal enhancement can be achieved.

Low chopper jitter with accurate tuneability, high frequency light modulation, and large slot/hole size are of great importance due to the mechanically resonant nature of the measurements, to achieve high spatial resolution and to allow a large wavelength range to be employed, respectively. We discuss each of these later in this section.

B. Setup for synchrotron infrared photothermal nanospectroscopy

The custom-made AFM-IR is based on our system thoroughly described by Donaldson *et al.*[1] In brief, the collimated synchrotron IR beam is first passed through an in-vacuum Michelson interferometer (Bruker Vertex 80v) to encode spectral information in the time domain. The IR beam passes in vacuum into the chopper box (blue lines in Fig. 5) and is focused through the chopper by a 90° off-axis parabolic mirror before being recollimated by a second off-axis parabola and exiting the vacuum system via a KBr window. The modulated IR light is passed to an optical microscope allowing precise focusing from below, through the substrate, onto the sample directly under the tip in the AFM (Nanonics MV1000) in contact mode.

A few details of the chopper setup are important to this method. The modulated synchrotron light is not directly detected in AFM-IR, so a reference laser is used in an optoswitch arrangement to provide the reference frequency and phase for the lock-in amplifier. The reference laser beam follows the red path shown in Fig. 5. The visible laser (FibreLyte LC, 635 nm, 10 mW CW from Global Laser) is located outside of the chopper box and is brought via a fiber-optic feedthrough into the vacuum chamber where it is focused through the same chopper hole as the IR beam. After the chopper, the laser beam is deflected onto the in-vacuum photodetector (PD in Fig. 5). The photodetector has a built-in preamplifier, and the generated reference signal is passed to the reference channel of the lock-in amplifier (Signal Recovery 7280).

By amplifying the components of the AFM-IR signal at different phases with respect to the optical modulation, it is possible either to probe the region directly below the AFM tip or to probe out-of-phase signals delayed due to thermal diffusion from regions away

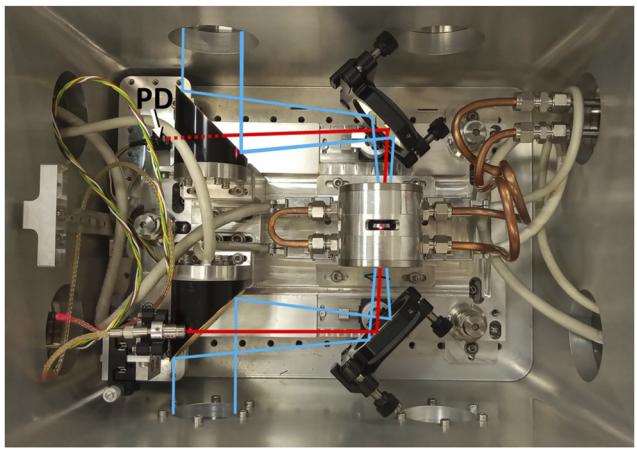

FIG. 5. Configuration of the water-cooled chopper and laser optoswitch in the vacuum box with optics. Blue line: SR beam path, red line: reference laser path, PD: photodiode with built-in amplifier.

from the tip, for example allowing subsurface detection of buried regions.

C. Jitter and frequency tuneability

By chopping the IR beam with low jitter at a contact resonance mode of the AFM cantilever, significant enhancements of the signal up to several orders of magnitude can be achieved depending on the quality factor of the resonance. With the addition of lock-in amplification to track the optical modulation and reject noise at other frequencies, the detection of the photothermal effect by the tip is remarkably sensitive, allowing measurements of nanometric sample volumes with picometer thermal expansion amplitudes. The lowest contact modes of typical Si cantilevers used lie in the range of 50–200 kHz and have sharp mechanical resonances with the full width at half maximum typically in the range of a few hundred Hz (quality factors >100) in air, depending on the nature of the sample.[23] If the jitter on the IR beam modulation is comparable to, or bigger than, the full width at half maximum of the contact resonance of the cantilever, then the cantilever resonance will not be driven efficiently, and the signal will be much weaker. In addition, the lock-in amplifier needs to able to tolerate the jitter coming from the optoswitch, otherwise the amplifier cannot lock to the signal and the photothermal effect is not detected.

When obtaining nanoscale spectral maps across heterogeneous samples, the contact resonance frequency can vary by much more than the linewidth (typically of order 10 kHz). This requires regular tuning of the chopper to match the contact resonance during the measurements, and the tuning speed is, therefore, important. The compact Celeroton rotor allows tuning up to 10 krpm s^{-1} (about 10 kHz s^{-1} for the 57-slot rotor) as standard, which is a major advantage of this system, making the time for chopper tuning very small compared with typical spectral measurement times of order minutes.

D. High frequency modulation

For photothermal nanospectroscopy measurements with a mechanically chopped broadband IR source, the probed region of the sample around the AFM tip depends on the timescale of local sample heating by the modulated IR beam and the thermal diffusion through the sample. Both the thermal diffusion volume and amplitude of thermal expansion in the sample decrease with increasing chopper modulation frequency as, for example, calculated by Donaldson *et al.*,[1] so that fast modulation leads to improved spatial resolution at the cost of signal intensity. Working in the resonance-enhanced mode at the lowest frequency (first) contact resonance of the AFM cantilever allows to probe a relatively large volume of the sample, while at the higher frequency second contact resonance, the photothermal signal comes from the smaller sample volume closer to the tip.

In Fig. 6, we compare spectroscopy performances with the first two contact resonances (65 and 190 kHz) of a gold coated probe with a hemispherical tip (HSC-60 Au, Team Nanotec). The sample was a homogeneous, 200 nm thick cyanoacrylate film (Loctite) deposited on a BaF_2 IR window (Crystran). The chopper rotation speed was optimized to modulate the beam at each frequency. In the first contact mode, the signal is much smaller and the only IR bands that can be appreciated above the noise are the intense C=O and C–O–O stretch modes around 1750 and 1250 cm^{-1}, respectively, while in the second contact mode, the spectrum is much stronger, and the full "fingerprint" region (below 2000 cm^{-1}) can be seen with high signal-to-noise ratio. Considering that the amplitude of thermal expansion is expected to be smaller for higher frequency modulation, the strong increase in signal from the second contact resonance suggests that the responsivity of the second resonance to expansion is much higher in these conditions. The background noise levels in the spectra measured at different contact resonances are quite similar. These results underline the rationale and importance of being able to modulate the IR beam at high frequencies for IR nanospectroscopy as made accessible by this novel chopper.

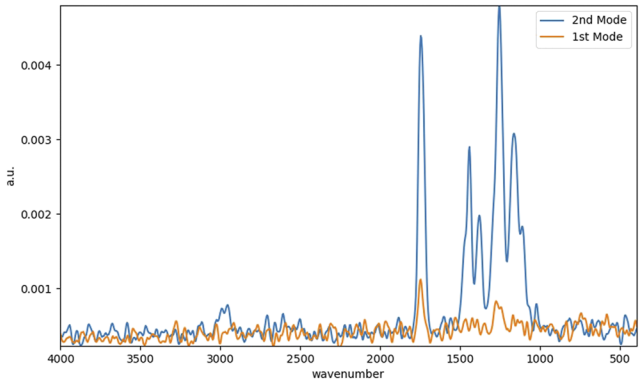

FIG. 6. AFM-IR spectra of a 200 nm thick cyanoacrylate film with the IR beam modulated at the first (~65 kHz, orange curve) and second cantilever contact resonance (~190 kHz, blue curve).

E. Importance of slot/hole size

The infrared light from the synchrotron[25] covers a very wide spectral range, including long wavelengths, which form a relatively large focal spot due to optical diffraction, and can, therefore, be easily clipped when passing through a small chopper hole. It is also important that all the wavelengths of the infrared are chopped in phase and that the maximum fraction of the beam power is modulated, i.e., ideally all the light is passing cleanly through a single hole. The 1 mm hole diameter was chosen to avoid clipping the IR beam when the chopper holes align with the beam.[4,12,15,18,26] Assuming an optically diffraction-limited focal spot size at the chopper, we can use the diameter of the Airy disk to estimate the longest wavelengths that would pass through the chopper without significant losses. For our optics size and focal length in the chopper box, a cutoff at a wavelength of circa 40 μm (250 cm^{-1}) is expected, which is in the far-IR range. To test that there is no cutoff due to the holes in the mid-IR range, the chopper rotor wheel was stopped and the spectrum of the light passing through the hole was obtained after refocusing onto a fast MCT detector (from Kolmar). The IR signal (Fig. 7) drops steadily below about 1000 cm^{-1} (above 10 μm wavelength), which is expected due to the sensitivity curve of the MCT detector, suggesting that the chopper holes are not limiting the optical throughput in this spectral range. Most of the visible synchrotron light was observed to pass through the chopper hole with no stray light through adjacent holes.

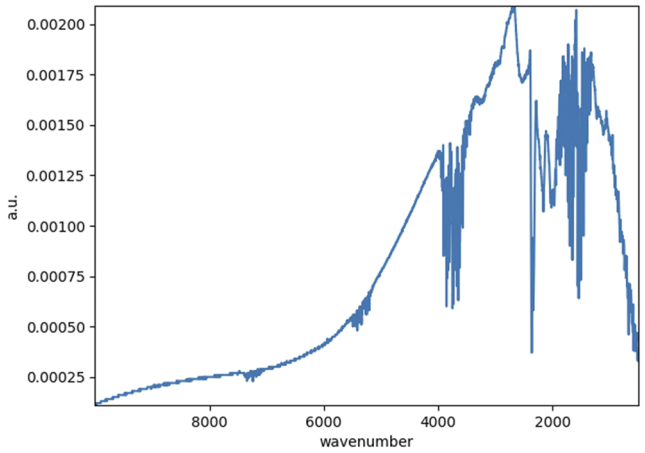

FIG. 7. IR spectrum of the full SR beam through one fixed chopper hole via MCT fast detector.

IV. CONCLUSIONS AND OUTLOOK

A new, magnetically levitated, mechanical chopper operating up to high speed with low jitter is described in this paper. Peak jitter below 1% is experimentally demonstrated at the highest modulation frequency of 200 kHz. The low jitter allows precision modulated optical measurements via lock-in detection at the desirable frequency, which can be tuned with an accuracy of 100 Hz. Detailed jitter analysis revealed that the size and position of the chopper holes dominated the peak jitter level, so that potentially, performances can be improved by a more precise and accurate mechanical manufacturing of the chopper blade. In our synchrotron nano-infrared spectroscopy application, the hole size of 1 mm introduces minimum clipping of the synchrotron IR beam even at the longest mid-IR wavelengths. The fast light modulation gives enhanced spectroscopy performance and new possibilities for challenging samples since it allows measurements below 200 nm sample thickness via the sensitive second contact resonance of the AFM cantilever, which was not possible with our previous low frequency mechanical chopper. The high tuning rate (10 kHz s^{-1}) of the compact rotor allows rapid frequency tuning for tracking the contact resonance when mapping heterogeneous samples, and in principle, this may be improved to as much as 50 kHz s^{-1} through optimization of the existing technology.

ACKNOWLEDGMENTS

This beamline upgrade project was funded by Diamond Light Source Limited (UK) and developed in collaboration with Celeroton AG (Switzerland). The authors would like to thank the following technical staff at Diamond for their contributions to the project: Andy Marshall and Avinash Kavva for mechanical design of the vacuum chamber and Steve Daniels and Lee Davidson for installation; Paul Roberts and Eugene Williams for electronics interfacing to the nano-infrared instrument; and Ed Warrick and Alessandro Evangelista for controls interfacing.

AUTHOR DECLARATIONS

Conflict of Interest

The authors declare no conflict of interest.

Author Contributions

Ioannis Lekkas: Data curation (equal); Investigation (equal); Methodology (equal); Writing – original draft (equal). **Mark D. Frogley**: Investigation (equal); Supervision (equal); Writing – original draft (equal); Writing – review & editing (lead). **Timon Achtnich**: Formal analysis (equal); Investigation (equal); Visualization (equal); Writing – original draft (equal). **Gianfelice Cinque**: Conceptualization (equal); Funding acquisition (lead); Investigation (equal); Methodology (equal); Supervision (equal); Writing – original draft (equal).

DATA AVAILABILITY

The data that support the findings of this study are available from the corresponding author upon reasonable request.

REFERENCES

[1] P. M. Donaldson, C. S. Kelley, M. D. Frogley, J. Filik, K. Wehbe, and G. Cinque, Opt. Express **24**, 1852 (2016).
[2] J. F. Holzman and A. Y. Elezzabi, Meas. Sci. Technol. **14**, N41 (2003).
[3] S. Plogmaker, P. Linusson, J. H. D. Eland, N. Baker, E. M. J. Johansson, H. Rensmo, R. Feifel, and H. Siegbahn, Rev. Sci. Instrum. **83**, 013115 (2012).
[4] V.-F. Duma, Lat. Am. J. Solids Struct. **10**, 5 (2013).
[5] H. Toshiyoshi, H. Fujita, and T. Ueda, in *Proceeding of IEEE Micro Electro Mechanical Systems: An Investigation of Micro Structures, Sensors, Actuators, Machines and Robotic Systems* (IEEE, 1994), p. 325.
[6] L. Li and D. Uttamchandani, in *IEE Proceedings - Science Measurement and Technology* (IET, 2004), Vol. 151.
[7] M. T. Ching, R. A. Brennen, and R. M. White, Opt. Eng. **33**, 3634 (1994).
[8] Y. Kogita, Y. Hirai, O. Tabata, and T. Tsuchiya, *2014 International Conference on Optical MEMS and Nanophotonics* (OPTICA, 2014), Vol. 65.
[9] H. Toshiyoshi, H. Fujita, and T. Ueda, J. Microelectromech. Syst. **4**, 3 (1995).
[10] P. E. McElligott, R. W. Roberts, and G. Jernakoff, Vacuum **13**, 419 (1963).
[11] M. Gembicky, D. Oss, R. Fuchs, and P. Coppens, J. Synchrotron Radiat. **12**, 665 (2005).
[12] D. F. Förster *et al.*, Opt. Lett. **40**, 2265 (2015).
[13] D. E. Voss and S. A. Cohen, J. Vac. Sci. Technol. **17**, 303 (1980).
[14] K. Ito *et al.*, Rev. Sci. Instrum. **80**, 123101 (2009).
[15] M. Cammarata *et al.*, Rev. Sci. Instrum. **80**, 015101 (2009).
[16] P. M. Selzer and W. M. Yen, Rev. Sci. Instrum. **47**, 749 (1976).
[17] J. Bhattacharyya, S. Ghosh, and B. M. Arora, Rev. Sci. Instrum. **76**, 083903 (2005).
[18] S. L. G. Husheer, J. M. Cole, T. d'Almeida, and S. J. Teat, Rev. Sci. Instrum. **81**, 043905 (2010).
[19] F. G. P. Seidl, D. J. Hughes, H. Palevsky, J. S. Levin, W. Y. Kato, and N. G. Sjöstrand, Phys. Rev. **95**, 476 (1954).
[20] G. W. Hoffmann and T. M. Jovin, Appl. Opt. **10**, 218 (1971).
[21] I. Mendaš, P. Vujković Cvijin, and D. Ignjatijević, Appl. Phys. B: Photophys. Laser Chem. **34**, 1 (1984).
[22] I. Mendaš and P. V. Cvijin, Appl. Phys. B: Photophys. Laser Chem. **32**, 119 (1983).

[23]M. D. Frogley, I. Lekkas, C. S. Kelley, and G. Cinque, Infrared Phys. Technol. **105**, 103238 (2020).
[24]K. L. A. Chan, I. Lekkas, M. D. Frogley, G. Cinque, A. Altharawi, G. Bello, and L. A. Dailey, Anal. Chem. **92**, 8097 (2020).
[25]G. Cinque, M. Frogley, K. Wehbe, J. Filik, and J. Pijanka, Synchrotron Radiat. News **24**, 24 (2011).
[26]V.-F. Duma, M. F. Nicolov, M. Kiss, T. Ilca, D. Demian, and L. Szantho, Proc. SPIE **8083**, 80830I (2011).